

NANO EXPRESS

Open Access



The CO₂ Storage Capacity of the Intercalated Diaminoalkane Graphene Oxides: A Combination of Experimental and Simulation Studies

Jing Xu¹, Wei Xing¹, Lianming Zhao^{1*}, Feifei Guo¹, Xiaozhong Wu¹, Wenbin Xu¹ and Zifeng Yan^{2*}

Abstract

To study the effect of interlayer spacing of pillared graphene oxides (GOs) on CO₂ uptake, we have obtained CO₂ isotherms with respect to the interlayer distance of pillared graphene oxide by both experimental and simulation methods. Interlayer distances of GO were modulated by intercalation of three kinds of diaminoalkanes with a different number of carbon atoms (NH₂(CH₂)_nNH₂, *n* = 4, 8, and 12) as pillars. The intercalated GOs (IGOs) and their reduced products (RIGOs) are characterized using a variety of approaches such as X-ray powder diffraction (XRD), Fourier transform infrared spectroscopy (FT-IR), X-ray photoelectron spectroscopy (XPS), and N₂ adsorption. Gas adsorption performance shows that the CO₂ uptake of IGOs and RIGOs decrease with the increase of the interlayer distance at low pressure, while at high pressure, the adsorption capacity of IGO-12 has a larger growth than those of both IGO-4 and IGO-8 and surpasses them at 30 bar. The contribution of the electrostatics to CO₂ adsorption is larger than that of van der Waals force at low pressures, whereas for the high pressures, the adsorption is dominated by van der Waals force.

Keywords: Intercalated graphite oxides; CO₂ adsorption; Grand canonical Monte Carlo simulation

Background

With the economic growth and industrial development, the excess fossil fuel combustion leads to a rapid increase of global warming and climate change. The rising atmospheric levels of CO₂ are considered to be responsible for the warming effect on the climate, because CO₂ emissions account for ca. 70 % of the gaseous irradiative force causing the greenhouse effect [1, 2]. Therefore, reducing the anthropogenic emission of CO₂ has recently become a political and technological priority [3]. Efficient CO₂ capture from existing emission sources plays a crucial role in reducing greenhouse gases in large quantities. However, CO₂ has a very low density under ambient conditions and thus is very difficult to be stored. Among various methods, adsorptive storage and capture of CO₂ by

physical adsorption in porous media is considered as an energetically efficient and technically feasible approach, where the gas sorption and storage capacity is mainly governed by a large accessible surface area and pore structure [4]. A wide variety of tailor-made porous materials, such as various carbon-based adsorbents (e.g., activated carbons [5, 6], carbon nanotubes [7, 8], and graphene [9]), zeolites [10, 11], and metal-organic frameworks (MOFs) [12, 13] have been proposed and studied for CO₂ storage application. Among them, graphene and graphene-based materials are considered as very promising candidates for the adsorption and storage of CO₂ [14] due to their unique properties such as large theoretical specific surface area and structural and chemical tenability. For example, Lee et al. reported an adsorption of 6.4 mmol g⁻¹ of CO₂ at 30 bar and 298 K on exfoliated graphene oxide (GO) with a specific surface area (SSA) of 547 m² g⁻¹ and a total pore volume of 2.47 cm³ g⁻¹ [15]. Mishra and Ramaprabhu found that a hydrogen-exfoliated graphene with a SSA

* Correspondence: lmzhao@upc.edu.cn; zfyancat@upc.edu.cn

¹College of Science, China University of Petroleum, Qingdao, Shandong 266580, People's Republic of China

²State Key Laboratory of Heavy Oil Processing, Key Laboratory of Catalysis, China University of Petroleum, Qingdao 266580, People's Republic of China

of $443 \text{ m}^2 \text{ g}^{-1}$ shows an enhanced CO_2 adsorption of 21.6 mmol g^{-1} at 11 bar and 298 K [16]. Meng and Park developed a kind of vacuum exfoliated graphene nanoplates with a high capture capacity, up to 56 mmol g^{-1} , at 30 bar and 298 K [17]. They also found that the improved CO_2 capture capacity of the graphene nanoplates is attributed to the larger interlayer spacing and higher interior void volume [17].

However, most of the pure graphene materials prepared seem very difficult to reach the theoretical specific surface area ($2600 \text{ m}^2 \text{ g}^{-1}$ [14]) and realize expanded graphene layers without any supports inserted between them. Therefore, pillaring of graphene or graphene oxide with organic ligands has been considered [18]. Recently, Zhou et al. designed and fabricated a porous graphene material by linking non-planar terpyridine complexes through an azide-alkyne click reaction [19]. This complex possesses high specific surface area of $440 \text{ m}^2 \text{ g}^{-1}$, and its carbon dioxide capacity could reach up to 2.6 mmol g^{-1} at 273 K and 1 atm. Burrell et al. [20] developed a novel pillared graphene oxide framework (GOF) material by cross-linking the benzenediboronic acids between GO layers. The GOF material shows the maximum interlayer distance of 1.05 nm and SSA of $470 \text{ m}^2 \text{ g}^{-1}$ and presents a good CO_2 adsorption of $\sim 2.7 \text{ mmol g}^{-1}$ at 4 bar and room temperature [20]. All these demonstrate that interlayer spacing of graphene-based materials could be tuned using pillaring molecules and thus remarkably influences their gas adsorption capacity. However, to the best of our knowledge, the investigations are rather scarce for dealing with the evolution of CO_2 adsorption properties with interlayer spacing of graphene-intercalated materials.

In this work, we investigated CO_2 uptake for a wide range of interlayer distances using the three-dimensional structure of GO obtained from intercalation of diaminoalkanes ($\text{H}_2\text{N}(\text{CH}_2)_n\text{NH}_2$). The interlayer spacing of intercalated composites was controlled precisely by adjusting the number of methylene units in $\text{H}_2\text{N}(\text{CH}_2)_n\text{NH}_2$ ($n = 4, 8, \text{ and } 12$). The effect of structural parameters of intercalated composites on their CO_2 adsorption properties was studied by a combination of experiment and grand canonical Monte Carlo (GCMC) simulation.

Methods

Experimental Section

Material Preparation

Graphite powder ($\sim 1.5 \mu\text{m}$) was purchased from Qingdao Ruisheng Graphite Co., Ltd. The diaminoalkanes were purchased from Aladdin Chemical Reagents Company. All others reagents were purchased from Shanghai Chemical Reagents Company and used as received. Graphite oxide was prepared according to a modified Hummers method [21]. GO suspension (6 mg ml^{-1}) was prepared by dispersing graphite oxide in deionized water under

ultrasonication for 1 h. The diaminoalkane-intercalated graphene oxides (IGOs) were synthesized according to Margarita's method [22]. In a typical synthesis, 4.16 mmol of 1, n -diaminooctane (where n represents the number of methylene units in diaminoalkanes) was dissolved into 35 mL of ethanol under stirring. The resulting solution was added into 33 ml of the as-prepared GO suspension under vigorous stirring at ambient temperature. The reaction continued for 48 h at room temperature with continuous stirring. Afterwards, the resulting solution was isolated by centrifugation, washed sequentially with deionized water/ethanol mixture (1:1 volume ratio) four times, then filtered, and dried in a vacuum oven at $80 \text{ }^\circ\text{C}$ for 24 h. The as-synthesized IGOs were then reduced by hydrazine hydrate at room temperature and dried at $50 \text{ }^\circ\text{C}$ under vacuum. The resultant was designated as reduced IGO (RIGOs).

Material Characterization

The interlayer distances of IGOs and RIGOs were examined by X-ray powder diffraction (XRD; PANalytical B.V., Netherlands) using a $\text{Cu K}\alpha_1$ radiation (0.15405 nm). The surface properties of the samples were characterized using Fourier transform infrared spectroscopy (FT-IR; Nicolet 6700, USA) and X-ray photoelectron spectroscopy (XPS; PHI 5000 VersaProbe, ULVAC-PHI, Japan). Nitrogen adsorption-desorption isotherms were measured at liquid nitrogen temperature (77 K) and CO_2 adsorption was performed at 273 K and 298 K using a surface area and porosity analyzer (ASAP2020M, Micromeritics, USA). The carbon samples were degassed under turbomolecular vacuum before sorption measurements. N_2 and CO_2 gases with super high purity (99.999 %) were used for the physisorption measurements. The Brunauer, Emmett, and Teller (BET) equation was used to calculate the apparent surface area from N_2 adsorption data obtained at P/P_0 between 0.05 and 0.2. For advanced porosity analysis, pore size distributions and cumulative pore volumes were determined by using non-local density functional theory (NLDFT) method considering sorption of CO_2 at 273 K in carbon as a model adsorbent and slit-like pores as a pore model. The implemented NLDFT model was supplied by the Quantachrome Autosorb ASiQwin 2.0 software. Note that microscopic methods based on statistical mechanics, such as NLDFT, which allow describing the configuration of the adsorbed phase on a molecular level, are currently considered as the more accurate method.

Theoretical Section

The Model Structure of IGOs

The periodic models of $[\text{C}_{36}\text{O}_2(\text{OH})_7(\text{HN}(\text{CH}_2)_4\text{NH})]_4$, $[\text{C}_{32}\text{O}(\text{OH})_5(\text{HN}(\text{CH}_2)_8\text{NH})]_4$, and $[\text{C}_{28}\text{O}(\text{OH})_3(\text{HN}(\text{CH}_2)_{12}\text{NH})]_4$ are representative of IGO- n ($n = 4, 8, \text{ and } 12$) structures, respectively (Additional file 1: Figure

S1). The chemical composition of the models was similar to that indicated by the experimental measurement of diaminoalkane, epoxy, and hydroxyl. The models were generated by using the periodic density functional theory (DFT) calculation, which were performed using the PW91 GGA functional with the double numerical basis set containing polarization functions (DNP) available in the DMol³ code packed in the Materials Studio (MS) 5.0 package [23, 24].

Interatomic Potentials

In this study, CO₂ molecule was represented by the conventional rigid linear triatomic model with three charged LJ interaction sites (C–O bond length of 0.1149 nm) centered on each atom as developed by Harris and Yung (see Additional file 1: Table S1) [25]. The interactions between the adsorbates and IGOs were described by a combination of site–site LJ and Coulombic potentials. In this work, the universal force fields (UFF) [26] (see Additional file 1: Table S1), which have been widely used to predict the thermodynamic and dynamic properties of various guests in graphene materials, were employed to model the atoms of IGOs. All the LJ cross-interaction parameters between the adsorbate/adsorbate and adsorbate/IGOs were determined by the Lorentz–Berthelot mixing rule, i.e., $\epsilon_{ij} = (\epsilon_{ii}\epsilon_{jj})^{1/2}$, $\sigma_{ij} = (\sigma_{ii} + \sigma_{jj})/2$.

Atomic Partial Charge for IGOs

The Mulliken charges were used to simulate the adsorption isotherms of CO₂ in the IGOs. These charges were obtained from the periodic DFT calculation, which were performed on the optimized unit cells of IGO using the PW91 GGA functional and the DNP basis set with the DMol³ code packed in the MS 5.0 package [23, 24].

Simulation Details

Grand canonical Monte Carlo (GCMC) simulations were conducted to explore the adsorption behaviors of CO₂ in the graphene using the MuSic code that was

developed by the Snurr group from the Western University (USA) [27]. For the simulations of CO₂, four types of attempts are considered: (i) insert, (ii) delete, (iii) transport, and (iv) rotate. The simulation box consisted of 8 (2 × 2 × 2) unit cells for the IGO-4, 24 (2 × 6 × 2) unit cells for the IGO-8, and 12 (3 × 2 × 2) unit cells for the IGO-12 materials. A cutoff radius of 1.2 nm was applied to the LJ interactions, while the long-range electrostatic interactions were handled by the Ewald summation method. Periodic boundary conditions (PBC) were considered in all the three dimensions. The Peng–Robinson equation of state was used to convert the pressure to the corresponding fugacity that was used in the GCMC simulations. For each state point, GCMC simulations consisted of 1 × 10⁷ steps to ensure the equilibration, followed by 1 × 10⁷ steps to sample the desired thermodynamic properties.

Results and Discussion

Physicochemical Properties

The XRD patterns of GO, IGOs, and RIGOs are shown in Fig. 1. As shown in Fig. 1, GO exhibits a strong and sharp diffraction peak at $2\theta = 11.9^\circ$, which corresponds to the diffraction of the (001) plane with an interplanar distance of 0.75 nm. The diffraction peak corresponding to the (002) plane of graphite at about $2\theta = 26.5^\circ$ is not observed, suggesting the complete oxidation of graphite. The oxidation of graphite leads to a large increase in the interplanar distance from about 0.34 to 0.75 nm. This is because oxygen-containing functional groups were attached to both sides of each graphene layer during oxidation. The reflection peaks of IGO-4, IGO-8, and IGO-12 appear at 10.8°, 9.1°, and 6.9°, respectively, exhibiting an increasing shift in the (001) peak position toward low angles. These suggest the one-dimensional expansion of the GO layers along its *c*-axis with an increased *d*-spacing as high as 0.82 (IGO-4), 0.97 (IGO-8), and 1.28 nm (IGO-12) (see Table 1). The significant increase of interlayer distances of IGOs indicates that the diaminoalkanes are

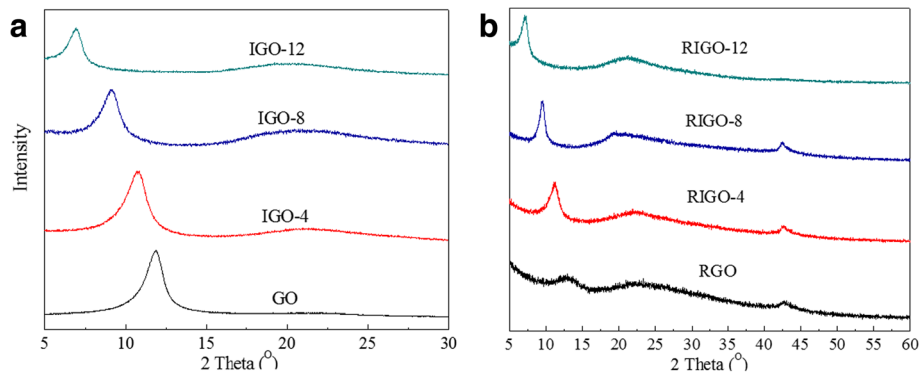


Fig. 1 XRD patterns of **a** GO and IGOs and **b** RGO and RIGOs

Table 1 Physicochemical properties of GO, RGO, IGOs, and RIGOs

Samples	XRD <i>d</i> -spacing (nm)	$S_{\text{BET}}^{\text{a}}$ ($\text{m}^2 \text{g}^{-1}$)	$S_{\text{mic}}^{\text{b}}$ ($\text{m}^2 \text{g}^{-1}$)	Cumulative pore volume of CO_2 ($\text{cm}^3 \text{g}^{-1}$)
GO	0.75	–	–	–
RGO	0.69	–	–	–
IGO-4	0.82	4.7	194.1	0.036
RIGO-4	0.79	14.0	334.7	0.053
IGO-8	0.97	10.6	138.4	0.022
RIGO-8	0.94	12.1	148.1	0.017
IGO-12	1.28	14.1	132.5	0.009
RIGO-12	1.24	26.1	118.5	0.008

^aBET surface area determined by N_2 sorption (77 K)

^bCumulative micropore surface area determined by CO_2 sorption (273 K) using the DFT method with a slit-shaped pore model

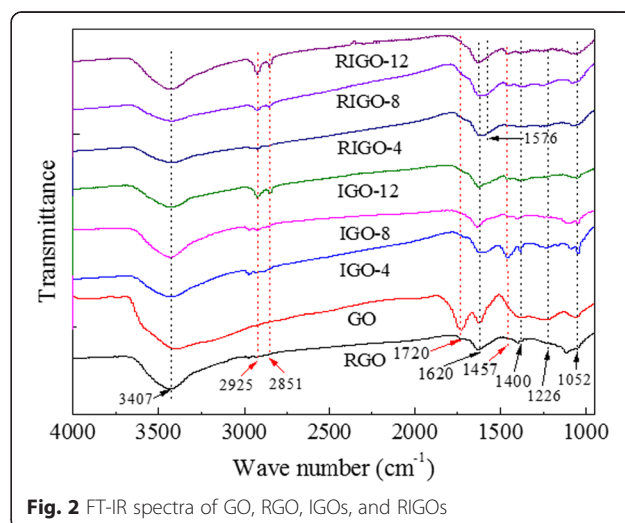
inserted into lamellar GO sheets. With the increase of methylene units in diaminoalkanes from 4 to 12, IGOs exhibit a gradually increasing and well-defined *d*-spacing between GO layers, suggesting that interplanar space is sensitive to the length of diaminoalkanes. In addition, it should be noted that the interlayer spacing is smaller than the theoretical size of intercalated diaminoalkanes, because the alkyl chains of intercalated diaminoalkanes may be bent and/or inclined.

To further modulate the interlayer distance, the reduction by hydrazine hydrate was performed at room temperature. As shown in Fig. 1, RIGOs show two new reflection peaks at 23° (002) and 42.4° (100), suggesting partial reduction of GO. The main reflection peaks of the RIGO-4, RIGO-8, and RIGO-12 appear at 11.3° , 9.5° , and 7.2° , with corresponding interplanar distances of 0.79, 0.94, and 1.24 nm (Table 1), respectively. The interplanar distances of RIGOs are slightly shorter than that of IGOs due to the removal of oxygen-containing groups that weaken the steric effect. However, the pillared structures of RIGOs are maintained after hydrazine reduction at room temperature.

FT-IR analyses are adopted to investigate the evolution of functional group during the intercalation of GO (see Fig. 2). For GO, one can see the following vibrational bonds: the broad O–H stretching vibration at 3407 cm^{-1} , the sharp C=O stretching vibration at 1720 cm^{-1} , the peak at 1400 cm^{-1} due to the O–H bending vibrations from hydroxyl group, and the peaks at 1226 and 1052 cm^{-1} corresponding to C–O stretching vibrations of epoxy and alkoxy. Furthermore, there is an additional peak located at 1620 cm^{-1} , which can be attributed to C=C stretching or skeletal vibrations of unoxidized graphitic domains. After intercalation of diaminoalkanes, IGOs show a clear, distinguishable additional IR mode at 1457, 2851, and 2925 cm^{-1} , corresponding to bending vibration, symmetric, and asymmetric stretching of the methylene groups ($-(\text{CH}_2)_n-$), respectively. All these further indicate that the diaminoalkanes are intercalated into the layers of GO. In addition, compared to GO, the peak intensity of C–O

and C=O groups of IGO decreases significantly, indicating that the GO surface functional groups were partially removed during the intercalation process. After reduction of IGOs, there is a new peak at 1576 cm^{-1} corresponding to the skeletal vibration of graphene sheets. This may be caused by the partial restoration of graphitic structure after hydrazine reduction.

The surface chemical properties for GO and IGOs were also revealed by XPS study Fig. 3 and Additional file 1: Figure S2. The full-range XPS analysis of GO clearly shows the presence of carbon (C) and oxygen (O) with atomic percentages of 69.7:30.3. The C 1s spectrum of GO can be deconvoluted into five peaks at 284.6, 285.0, 286.7, 287.6, and 289.0 eV (Additional file 1: Figures S2 and Table S3), corresponding to C=C/C–C in aromatic rings, C–O in alkoxy groups, O–C–O in epoxy groups, C=O in carbonyl groups, and O–C=O in carboxyl groups, respectively. After intercalation of diaminoalkanes, the peak intensity of O–C–O in IGOs decreased sharply, whereas that of the C–OH species increased (see Fig. 3). Concurrently, the two new peaks for C–N and N–C(O) bonds appear as shown in the C 1s spectra, corroborating

**Fig. 2** FT-IR spectra of GO, RGO, IGOs, and RIGOs

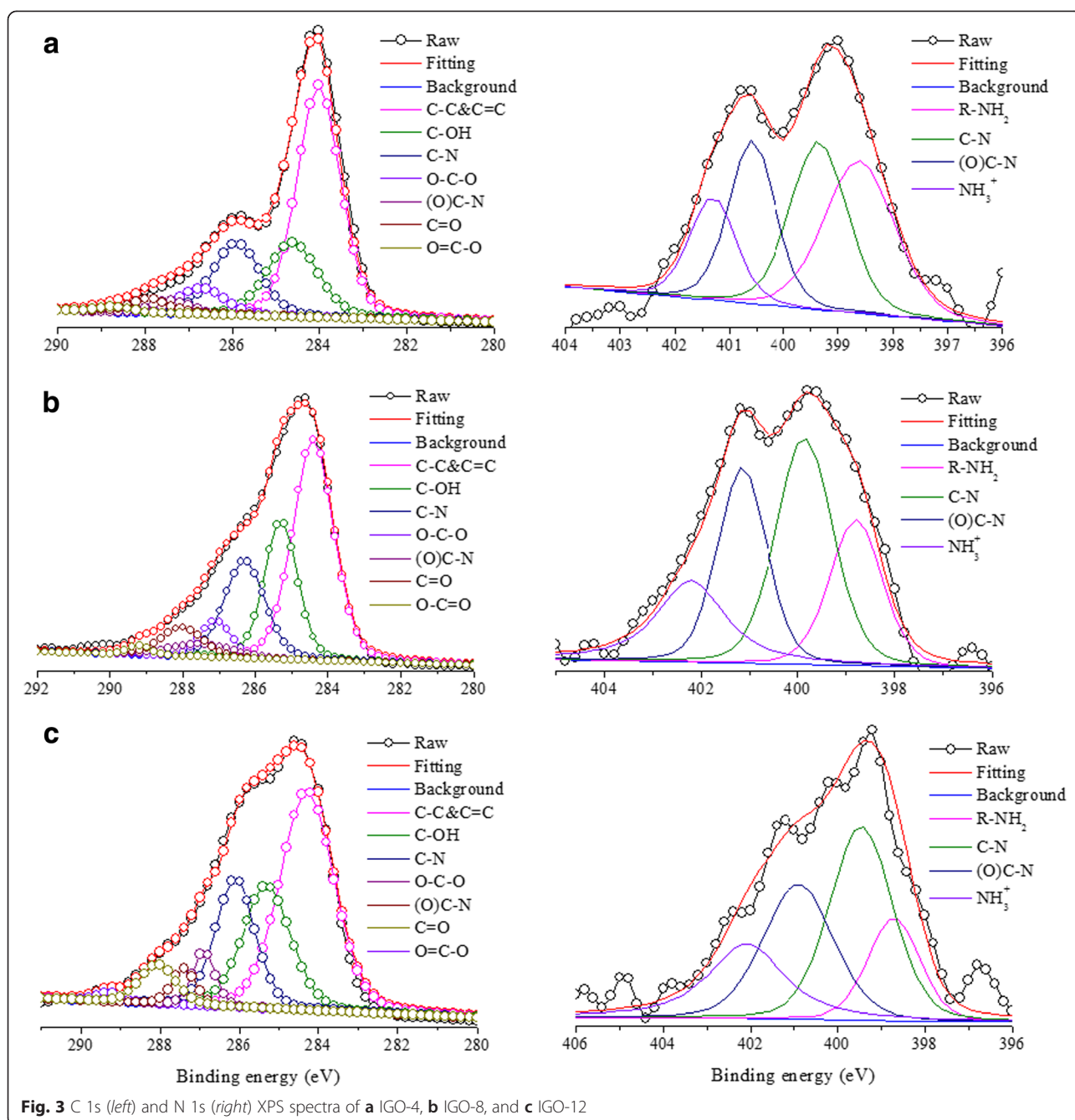


Fig. 3 C 1s (left) and N 1s (right) XPS spectra of **a** IGO-4, **b** IGO-8, and **c** IGO-12

with its N 1s XPS spectra and suggesting that a covalent bond-forming reaction has occurred. This behavior can be understood via the mechanism suggested by Burlinos [28], where alkylamine could readily react with graphene oxide via nucleophilic attack of amine on epoxide group. Interestingly, with the increase of the number of methylene in pillaring units, the content of C–OH species increases gradually, but that of C–O–C species decreases (Table 2). This can be attributed to the different lengths of diaminoalkanes ($n = 4, 8, \text{ and } 12$) and their possible

conformations between GO layers. With the increase of the length of alkyl chains, there is a larger probability of amines binding with epoxide groups on GO, forming formbridge or loop conformations. This situation is also supported by the N 1s XPS spectra, where the C–N and (O)C–N species increase and the R–NH₂ groups decrease with the number of methylene increasing in diaminoalkanes (Table 3). A weak alkylammonium ion (C–NH₃⁺) peak is also present in the N 1s spectra of IGOs, which originated from the association of amine

Table 2 The C 1s XPS spectra of IGOs

Bonds	Peak area		
	IGO-4 (%)	IGO-8 (%)	IGO-12 (%)
C-C/C=C	50	44	45
C-OH	19	22	23
C-N	17	20	20
C-O-C	6	5	4
N-C(O)	2	4	3
C=O	3	5	5
O-C=O	1	1	1

with the small number of carboxylate groups on the edges of the graphene oxide sheets, as proposed by Matsuo et al. [29]. In addition, for IGO-*n* (*n* = 4, 8, and 12), the atomic ratio of C, N, and O is found to be 76.2:3.7:20.1, 78.7:4.0:17.3, and 81.6:3.6:14.9, respectively, suggesting that a ratio of graphene C, diaminoalkane pillar, and oxygen-containing group is about 37.0:1:10.8, 31.3:1:8.6, and 29.7:1:4.7, respectively.

Nitrogen adsorption experiments (at 77 K) were performed to examine the surface textural characteristics. Fig. 4a shows the N₂ adsorption-desorption isotherms, which fall in between I- and IV-type isotherms. At low relative pressure, the adsorption amount rapidly increases, suggesting the existence of micropores in IGOs. On the other hand, the H1 and H2 hysteresis loops and the durative increase of the adsorption capacity at *P* > 40 kPa for IGOs reveal the presence of meso/macropores formed by accumulation of IGO sheets. When the number of methylene units in diaminoalkanes rises from 4 to 8, and to 12, the amount of adsorbed N₂ at 1 atm gradually increases from 0.42 to 1.30 and then to 1.54 mmol g⁻¹, respectively. The corresponding BET surface areas increase from 4.7 m² g⁻¹ for IGO-4, to 10.6 m² g⁻¹ for IGO-8, and to 14.1 m² g⁻¹ for IGO-12 (Table 1). After hydrazine reduction, the adsorption capacity of N₂ in the RIGOs increases slightly. The N₂ uptake at 1 atm increases to 1.52 mmol g⁻¹ for RIGO-4, to 2.92 mmol g⁻¹ for RIGO-8, and to 9.00 mmol g⁻¹ for RIGO-12, and the corresponding BET surface area is found to be 14.0, 12.1, and 26.1 m² g⁻¹, respectively.

Table 3 The N 1s XPS spectra of IGOs

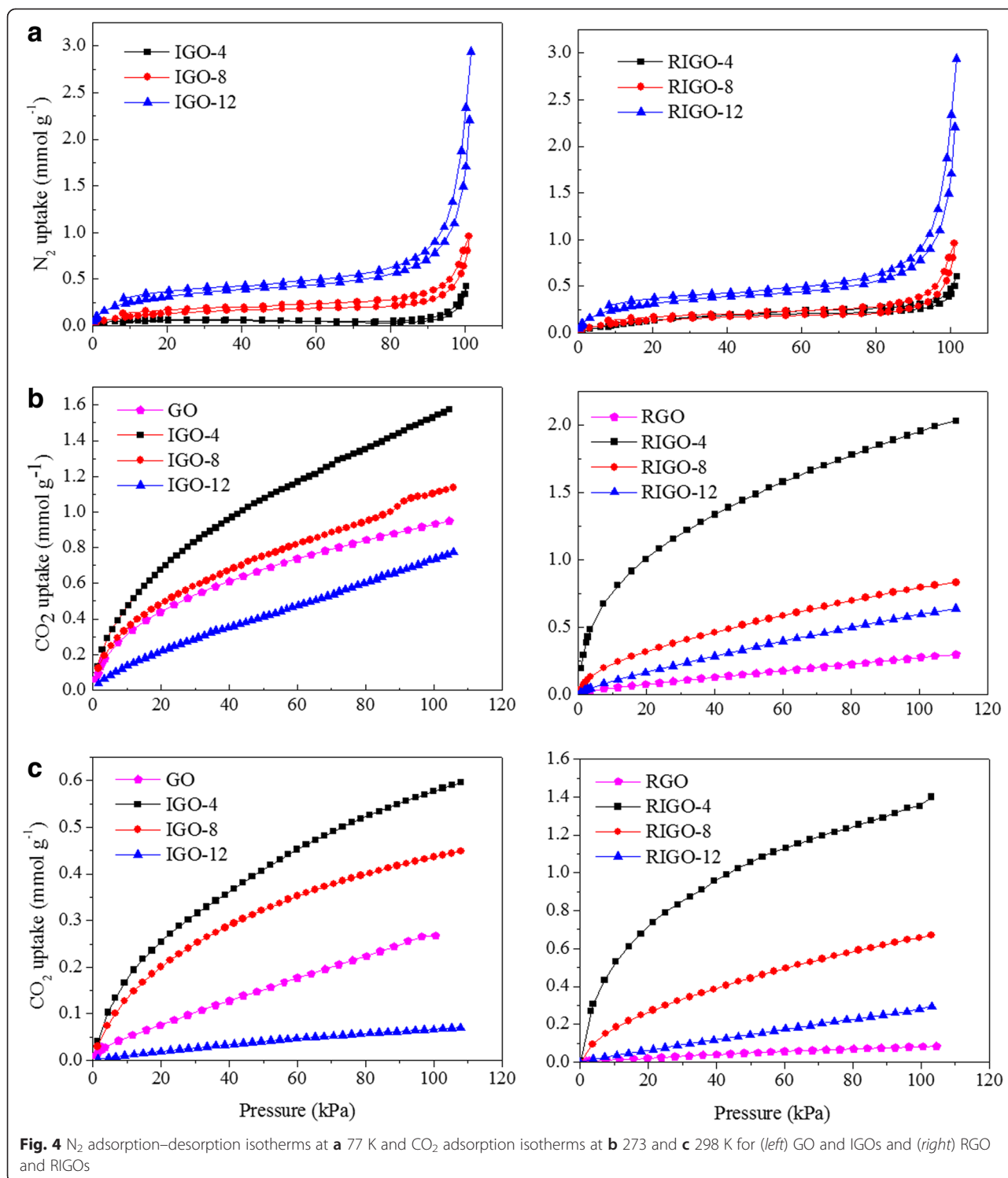
Bonds	Peak area		
	IGO-4 (%)	IGO-8 (%)	IGO-12 (%)
R-NH ₂	32	20	15
C-N	29	34	35
(O)C-N	23	26	28
C-NH ₃ ⁺	14	18	20

CO₂ Capture Performances

The CO₂ adsorption performances were measured at 273 and 298 K under the pressure of 0~1 atm (see Fig. 4). In contrary to the adsorption of N₂, the total CO₂ uptake follows the order of IGO-4 (~1.54 mmol g⁻¹ at 1 atm) > IGO-8 (~1.11 mmol g⁻¹) > GO (~0.93 mmol g⁻¹) > IGO-12 (~0.74 mmol g⁻¹) at 273 K (see Fig. 4b). Compared with GO, intercalation of a short pillar ((NH₂(CH₂)_{*n*}NH₂, *n* = 4 and 8) is found to promote the absorption of CO₂, while a high pillar ((NH₂(CH₂)₁₂NH₂) has an unfavorable effect on the CO₂ absorption. The corresponding micropore surface areas for IGO-*n* (*n* = 4, 8, and 12) are found to be 194.1, 138.4, and 132.5 m² g⁻¹, respectively, which are much larger than those determined by N₂ adsorption. This suggests that some ultramicropores in the interlayer space could be probed by CO₂ molecules but N₂ molecules, due to a smaller kinetic diameter of CO₂ (0.33 nm) than N₂ (0.36 nm) and a high kinetic energy for CO₂ diffusion at 273 K. It has been well documented that microporosity plays a key role in CO₂ adsorption on various carbon materials. The pore size distribution of IGOs was obtained by using the NLDFT method (Fig. 5). Among three IGOs, the IGO-4 has the broadest micropore size distribution in the range of 0.45–0.87 nm, followed by IGO-8 (0.45–0.82 nm), and IGO-12 (0.45–0.78 nm). The cumulative pore volume decrease from 0.036 cm³ g⁻¹ (IGO-4) to 0.022 cm³ g⁻¹ (IGO-8) to 0.009 cm³ g⁻¹ (IGO-12), respectively (Table 1 and Additional file 1: Figure S3). The CO₂ uptake presents a good correlation with the volume and surface area of ultramicropores. Our observation is also consistent with recent studies on a series of carbon materials that showed enhanced CO₂ uptake for samples having micropores below 0.7 nm [30–32], where CO₂ adsorption inside these pores takes place by micropore filling instead of layer by layer adsorption. The declined tendency of micropores for IGO-*n* (*n* = 4, 8, and 12) may be due to the increase of the interplanar space and the decrease of the oxygen-containing functional groups.

After hydrazine reduction, the micropore surface area determined by CO₂ adsorption is found to be 334.7, 148.1, and 118.5 m² g⁻¹ for RIGOA-*n* (*n* = 4, 8, and 12), respectively, and the corresponding CO₂ uptake capacity reaches as high as 1.97, 0.80, 0.60 mmol g⁻¹ at 1 atm and 273 K. For RIGOA-*n* (*n* = 4, 8, and 12), all their CO₂ uptake capacities are larger than that of RGO (~0.28 mmol g⁻¹ at 1 atm and 273 K). When the temperature increases to 298 K, the CO₂ adsorption capacity decreases for both IGO-*n* (0.58, 0.44, and 0.07 mmol g⁻¹ at 1 atm for *n* = 4, 8, and 12, respectively) and RIGO-*n* (1.37, 0.66, and 0.29 mmol g⁻¹).

CO₂ adsorption in IGOs was also simulated with the Mulliken charges on framework atoms. An atomistic representation of IGOs was built using a DFT computational-assisted structure determination, as described in the



“Methods” section. Figure 6 and Additional file 1: Figure S4 present the calculated excess and absolute adsorption isotherms at 273 K using GCMC simulations. It can be seen that the difference between the absolute and excess isotherms increases monotonically at low pressure and tends to flatten out to a constant value of 0.5, 0.8, and

1.0 mmol g⁻¹ at 30 bar for IGO-*n*, *n* = 4, 8, and 12, respectively. The largest difference for IGO-12 is attributed to its relatively largest free volume as presence of the maximum interplanar space among three IGOs. At the pressure below 1 atm, the calculated excess adsorption isotherms of CO_2 are according well with those measured

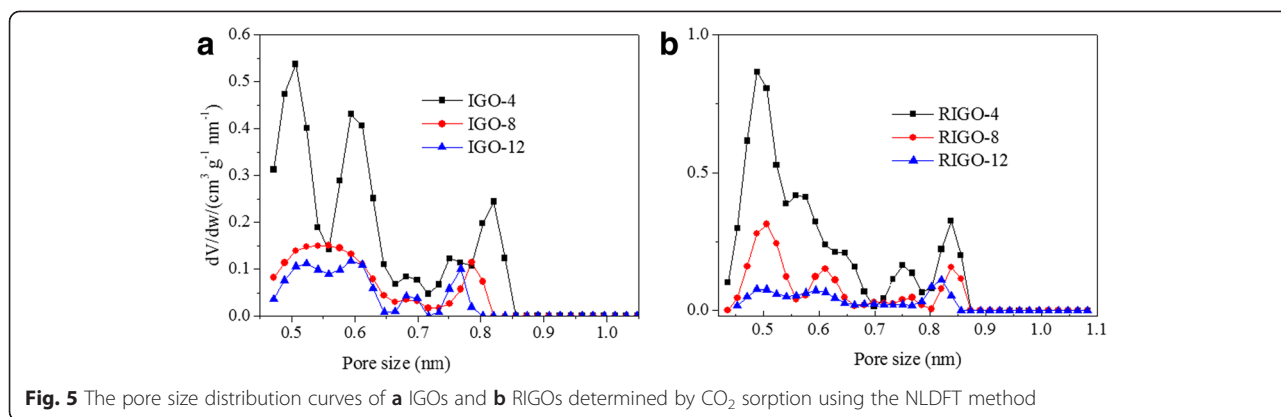


Fig. 5 The pore size distribution curves of **a** IGOs and **b** RIGOs determined by CO₂ sorption using the NLDFT method

by experiment with a standard deviation of about 0.06 mmol g⁻¹, which validates the force fields and models used. The deviation may be attributed to crystal imperfections and presence of solvent molecules inside the pores in synthesized structures. With the increase of pressure, the simulated CO₂ uptake increases for all IGOs, especially IGO-12. Indeed, the CO₂ uptake in IGO-12 is even greater than those in both IGO-4 and IGO-8 at 30 bar, and up to 3.68 mmol g⁻¹ at 35 bar compared with 3.54 and 2.87 mmol g⁻¹ for IGO-4 and 8, respectively. As shown in Fig. 6, CO₂ uptake of IGO-*n* changes gradually from I- to II-type isotherms for *n* = 4, 8, and 12. Unlike low-pressure uptake which is mostly governed by ultramicropores, large micropores and narrow mesopores are the predominant attributes for attaining high storage capacities at elevated pressures [30, 33]. With the increase of interlayer spacing and decrease of oxygen-containing groups for IGO-*n*, *n* = 4, 8, and 12, the amount of large micropores and narrow mesopores may increase, leading to a larger increase of CO₂ uptake for IGO-12 than both IGO-4 and IGO-8.

To investigate the CO₂/IGO surface interactions, the isosteric heats of adsorption (*Q_{st}*) were calculated by the virial method using CO₂ adsorption isotherms collected at 273 and 298 K (Fig. 7) [34]. The *Q_{st}* value reflects the interaction strength between CO₂ and IGOs. At a low pressure, the CO₂ adsorption on IGOs presents high *Q_{st}* (about 37–47 kJ mol⁻¹), indicating that the surface of IGOs strongly interacts with CO₂ molecules, which is attributed to the strong adsorption property of oxygen-containing functional groups on IGO sheets [35]. With increasing sorption pressure, the curves of *Q_{st}* show a drop, indicating a decrease of interaction strength between the IGOs and CO₂ as intermolecular interaction of adsorbates with the filling of CO₂. Furthermore, the value of *Q_{st}* follows the order of IGO-4 > IGO-8 > IGO-12, suggesting that CO₂ molecules interact most strongly with IGO-4, followed by IGO-8, and then IGO-12. This further indicates that a smaller interlayer spacing favors the CO₂ uptake, due to the stronger superposition of the van der Waals force given by two adjacent walls [32].

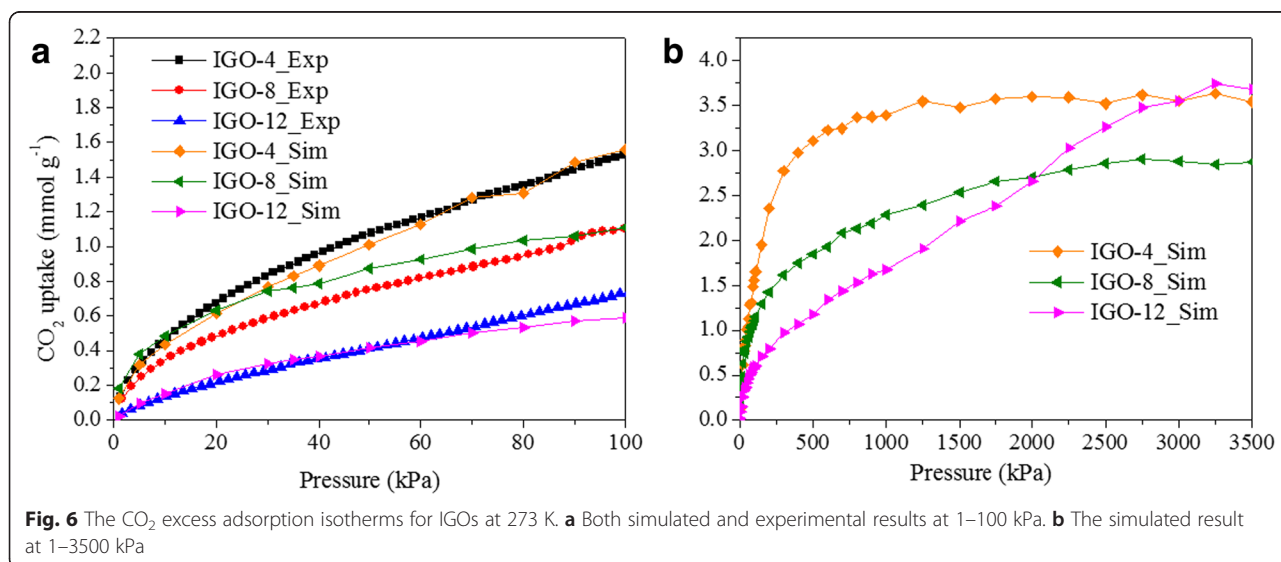
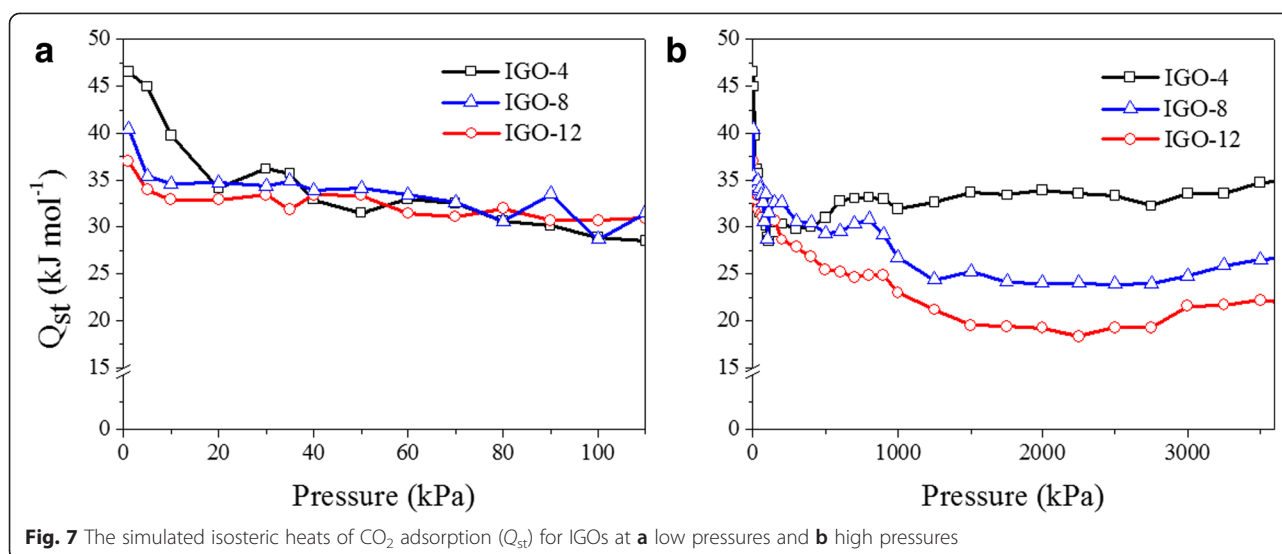


Fig. 6 The CO₂ excess adsorption isotherms for IGOs at 273 K. **a** Both simulated and experimental results at 1–100 kPa. **b** The simulated result at 1–3500 kPa



To further illustrate the effect of electrostatic and van der Waals (non-electrostatic) interactions on CO₂ uptake, additional simulations were conducted by eliminating the contribution of electrostatic interaction (Fig. 8). As shown in Fig. 8, for IGO-4, the contribution of the electrostatics to the CO₂ adsorption is relatively large (about 55–65 %) at low pressures and found to be maximum at 0.6 bar. Then, its contribution to adsorption decreases monotonically, contributing a few percent (about 10–14 %) at pressures above 15 bar. Overall, in the presence of electrostatic interaction, the CO₂ amount adsorbed is about 120–190 % higher than that given by the LJ core alone under low pressures, whereas the adsorption is dominated by the van der Waals force under high pressures.

Conclusions

We investigated the effect of interlayer spacing on CO₂ uptake for pillared graphene oxides by both experimental and

simulation methods. Interlayer distances of GO were tuned by intercalation of three diaminoalkanes (NH₂(CH₂)_{*n*}NH₂, *n* = 4, 8, and 12) with different lengths of alkyl chain. At low pressures, the CO₂ adsorption capacity of IGOs decreases with the increase of the interlayer distance, where the electrostatic interaction of adsorbent has a larger contribution to the adsorption than van der Waals force. As the pressure increases, CO₂ uptake of IGO-12 increases sharply and surpasses those of both IGO-4 and IGO-8 at 30 bar, where the van der Waals force plays a dominant role. This new finding demonstrates that the modulation of interlayer spacing of pillared graphene oxides could enhance their CO₂ adsorbability, which provides useful information to design graphene-based materials with superior CO₂ adsorption capacity.

Additional file

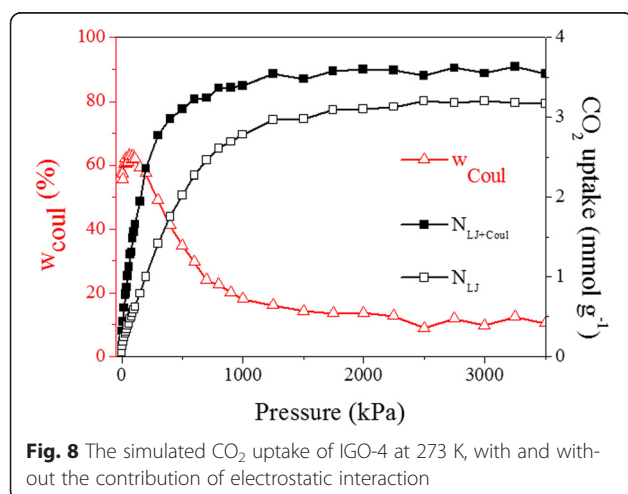
Additional file 1: Figure S1. The optimized models of (a) IGO-4, (b) IGO-8, (c) IGO-12. **Figure S2.** The C 1s XPS spectra of GO. **Figure S3.** The cumulative pore volume curves of (a) IGOs and (b) RIGOs determined by CO₂ sorption. **Figure S4.** The simulated CO₂ absolute adsorption isotherms for IGOs at 273 K. **Table S1.** Interatomic potential parameters and partial charges for CO₂ molecule. **Table S2.** Interatomic potential parameters (from the UFF force field) for the atoms in IGOs. **Table S3.** The C 1s XPS spectra of GO.

Competing interests

The authors declare that they have no competing interests.

Authors' contributions

JX and Wix contributed equally in this paper and they performed the experiments and drafted the manuscript together. WnX and LZ performed the CO₂ adsorption simulation. FG checked the figures and gave the final approval of the version to be published. XW performed the partial experiments. ZY guided the idea and revised and finalized the manuscript. All authors read and approved the final manuscript.



Acknowledgements

This work was supported by the National Natural Science Foundation of China (51107076), Distinguished Young Scientist Foundation of Shandong Province (JQ201215), Natural Science Foundation of Shandong Province (ZR2015BQ009), Taishan Scholar Foundation (ts20130929), Promotive Research Fund for Excellent Young and Middle-aged Scientists of Shandong Province (BS2012NJ015), and Fundamental Research Funds for the Central Universities (12CX02014A and 15CX08010A).

Received: 18 June 2015 Accepted: 28 July 2015

Published online: 08 August 2015

References

- Van der Hoeven M. CO₂ emissions from fuel combustion: highlights. Paris: Organisation for Economic Co-operation and Development/International Energy Agency (OECD/IEA); 2012.
- Pachauri RK, Reisinger A, eds. Fourth assessment report on climate change. Intergovernmental Panel on Climate Change (IPCC), Geneva, Switzerland; 2007.
- UNFCCC Kyoto Protocol, revised 2013. http://unfccc.int/kyoto_protocol/items/2830.php. Accessed 1 May 2013.
- Xiang ZH, Cao DP, Lan JH, Wang WC, Broom DP. Multiscale simulation and modelling of adsorptive processes for energy gas storage and carbon dioxide capture in porous coordination frameworks. *Energy Environ Sci*. 2010;3:1469–87.
- Wickramaratne NP, Jaroniec M. Activated carbon spheres for CO₂ adsorption. *ACS Appl Mater Interfaces*. 2013;5:1849–55.
- Silvestre-Albero A, Silvestre-Albero H, Martínez-Escandell M, Rodríguez-Reinoso F. Micro/mesoporous activated carbons derived from polyaniline: promising candidates for CO₂ adsorption. *Ind Eng Chem Res*. 2014;53:15398–405.
- Liu Q, Shi JJ, Zheng SD, Tao MN, He Y, Shi Y. Kinetics studies of CO₂ adsorption/desorption on amine-functionalized multiwalled carbon nanotubes. *Ind Eng Chem Res*. 2014;53:11677–83.
- Quiñero D, Frontera A, Deyà PM. Feasibility of single-walled carbon nanotubes as materials for CO₂ adsorption: a DFT study. *J Phys Chem C*. 2012;116:21083–92.
- Xu SC, Irle S, Musaev DG, Lin MC. Quantum chemical prediction of reaction pathways and rate constants for dissociative adsorption of CO_x and NO_x on the graphite (0001) surface. *J Phys Chem B*. 2006;110:21135–44.
- Dunne LJ, Furgani A, Jalili S, Manos G. Monte-Carlo simulations of methane/carbon dioxide and ethane/carbon dioxide mixture adsorption in zeolites and comparison with matrix treatment of statistical mechanical lattice model. *Chem Phys*. 2009;359:27–30.
- Martin-Calvo A, Parra JB, Ania CO, Calero S. Insights on the anomalous adsorption of carbon dioxide in LTA zeolites. *J Phys Chem C*. 2014;118:25460–7.
- Tranchemontagne DJ, Ni Z, O'Keeffe M, Yaghi OM. Reticular chemistry of metal-organic polyhedra. *Angew Chem Int Ed*. 2008;47:5136–47.
- Liu B, Wu WP, Hou L, Wang YY. Four uncommon nanocage-based Ln-MOFs: highly selective luminescent sensing for Cu²⁺ ions and selective CO₂ capture. *Chem Commun*. 2014;50:8731–4.
- Gadipelli S, Guo ZX. Graphene-based materials: synthesis and gas sorption, storage and separation. *Prog Mater Sci*. 2015;69:1–60.
- Lee SY, Park SJ. Isothermal exfoliation of graphene oxide by a new carbon dioxide pressure swing method. *Carbon*. 2014;68:112–7.
- Mishra AK, Ramaprabhu S. Carbon dioxide adsorption in graphene sheets. *AIP Adv*. 2011;1:032152.
- Meng LY, Park SJ. Effect of exfoliation temperature on carbon dioxide capture of graphene nanoplates. *J Colloid Interface Sci*. 2012;386:285–90.
- Garberoglio G, Pugno NM, Taioli S. Gas adsorption and separation in realistic and idealized frameworks of organic pillared graphene: a comparative study. *J Phys Chem C*. 2015;119:1980–7.
- Zhou D, Cheng QY, Cui Y, Wang T, Li X, Han BH. Graphene-terpyridine complex hybrid porous material for carbon dioxide adsorption. *Carbon*. 2014;66:592–8.
- Burruss JW, Gadipelli S, Ford J, Simmons JM, Zhou W, Yildirim T. Graphene oxide framework materials: theoretical predictions and experimental results. *Angew Chem Int Ed*. 2010;49:8902–4.
- Hummers Jr WS, Offeman RE. Preparation of graphitic oxide. *J Am Chem Soc*. 1958;80:1339.
- Herrera-Alonso M, Abdala AA, McAllister MJ, Aksay IA, Prud'homme RK. Intercalation and stitching of graphite oxide with diaminoalkanes. *Langmuir*. 2007;23:10644–9.
- Delley B. From molecules to solids with the Dmol³ approach. *J Chem Phys*. 2000;113:7756–64.
- Delley B. Fast calculation of electrostatics in crystals and large molecules. *J Phys Chem*. 1996;100:6107–10.
- Harris JG, Yung K. Carbon dioxide's liquid-vapor coexistence curve and critical properties as predicted by a simple molecular model. *J Phys Chem*. 1995;99:12021–4.
- Rappé AK, Casewit CJ, Colwell KS, Goddard III WA, Skiff WM. UFF, a full periodic table force field for molecular mechanics and molecular dynamics simulations. *J Am Chem Soc*. 1992;114:10024–35.
- Gupta A, Chempath S, Sanborn MJ, Clark LA, Snurr RQ. Object-oriented programming paradigms for molecular modeling. *Mol Simulat*. 2003;29:29–46.
- Bourlinos AB, Gournis D, Petridis D, Szabo T, Szeri A, Dekany I. Graphite oxide: chemical reduction to graphite and surface modification with primary aliphatic amines and amino acids. *Langmuir*. 2003;19:6050–5.
- Matsuo Y, Miyabe T, Fukutsuka T, Sugie Y. Preparation and characterization of alkylamine-intercalated graphite oxides. *Carbon*. 2007;45:1005–12.
- Ashourirad B, Sekizkardes AK, Altarawneh S, El-Kaderi HM. Exceptional gas adsorption properties by nitrogen-doped porous carbons derived from benzimidazole-linked polymers. *Chem Mater*. 2015;27:1349–58.
- Pevida C, Drage TC, Snape CE. Silica-templated melamine-formaldehyde resin derived adsorbents for CO₂ capture. *Carbon*. 2008;46:1464–74.
- Zhang Z, Zhou J, Xing W, Xue Q, Yan Z, Zhuo S, et al. Critical role of small micropores in high CO₂ uptake. *Phys Chem Chem Phys*. 2013;15:2523–9.
- Casco ME, Martínez-Escandell M, Silvestre-Albero J, Rodríguez-Reinoso F. Effect of the porous structure in carbon materials for CO₂ capture at atmospheric and high-pressure. *Carbon*. 2014;67:230–5.
- Vuong T, Monson PA. Monte Carlo simulation studies of heats of adsorption in heterogeneous solids. *Langmuir*. 1996;12:5425–32.
- Xing W, Liu C, Zhou ZY, Zhou J, Wang GQ, Zhuo SP, et al. Oxygen-containing functional group-facilitated CO₂ capture by carbide-derived carbons. *Nanoscale Res Lett*. 2014;9:189–96.

Submit your manuscript to a SpringerOpen® journal and benefit from:

- Convenient online submission
- Rigorous peer review
- Immediate publication on acceptance
- Open access: articles freely available online
- High visibility within the field
- Retaining the copyright to your article

Submit your next manuscript at ► springeropen.com